A 3D Geometry-based Stochastic Channel Model for UAV-MIMO Channels

Linzhou Zeng[1,2], Xiang Cheng[1,2], Cheng-Xiang Wang[3,4], and Xuefeng Yin[5]
[1]State Key Laboratory of Advanced Optical Communication Systems and Networks,
School of Electronics Engineering and Computer Science, Peking University, Beijing, 100871, China
[2]National Mobile Communications Research Laboratory, Southeast University, Nanjing, 210096, China
[3]School of Engineering and Physical Sciences, Heriot-Watt University, Edinburgh, EH14 4AS, UK
[4]Shandong Provincial Key Lab of Wireless Communication Technologies, Shandong University, Jinan, 250100, China
[5]College of Electronics and Information Engineering, Tongji University, Shanghai, 201804, China
Email: {linzhou.zeng, xiangcheng}@pku.edu.cn, cheng-xiang.wang@hw.ac.uk, yinxuefeng@tongji.edu.cn

***Abstract*—Unmanned Aerial Vehicles (UAVs) have been a promising platform in realizing high-speed wireless networks. As an emerging scenario, the UAV communication is distinct from widely used cellular systems or vehicular networks, requiring the development of practical yet easy-to-use channel models. In this paper, for the first time we introduce the geometry-based stochastic model (GBSM) to UAV channel modeling, and propose a new three-dimensional (3D) GBSM for UAV Multi-Input Multi-Output (UAV-MIMO) channels. Based on the proposed model, we derive and investigate the space-time correlation function (STCF) under a 3D moving and scattering environment. The usefulness of this model is verified by the comparison between the theoretical results and some measurement data.**

I. Introduction

UAVs, also called drones, have found a wide range of applications in the past decade. Despite their primary deployment in the military, UAVs are now more accessible to the public with the cost reduction and device miniaturization. Therefore, various civillian applications have emerged, such as cargo transport, emergency rescue, and communication relay. Among these applications, the utilization towards high-speed wireless communications has received much attention, where MIMO techniques can further improve the performance [1]. The UAV communication is a brand new scenario in terms of propagation environments, and thus the corresponding channel characteristics differ from those in cellular and vehicular communications. Therefore, it is desirable to develop UAV-MIMO channel models to serve the system design [2].

Since the UAV communication is a newly emerging scenario, corresponding channel measurements and modeling are still in its infancy. Only several researchers developed UAV channel measurement campaigns [3]-[6], while the channel-modeling-related work is even less. Several deterministic channel modeling approaches have been applied to UAV channels, including the ray-tracing method [7] and the finite difference time domain (FDTD) method [8]. Every specific application of these approaches is based on numerous physical data and strictly confined to the corresponding environment, which leads to both high complexity and limited generality. Alternatively, some researchers have focused on the development of stochastic models, which have lower complexity and can be easily generalized to various UAV scenarios with acceptable accuracy. These stochastic models can be classified into the statistical model [9] and the curved-earth two-ray (CE2R) model [10]. The statistical model (Rayleigh or Ricean process) was classical in wireless channel modeling, but not capable of capturing some unique features of UAV communications, e.g., the UAV's mobility and altitude. The CE2R model was designed for large-UAV scenarios, where the ground curvature is appreciable, and the propagation is dominated by a line-of-sight (LoS) path and a ground reflection. Therefore, it cannot be used for popular small-UAV scenarios. Unlike the above stochastic modeling approaches, another well-known one, namely the GBSM approach [11], characterizes the multipath channels by applying simplified ray-tracing rules on effective scatterers that are randomly distributed in a geometry. The GBSM has been widely used for modeling the cellular or vehicular channels due to its high accuracy and low complexity [12]-[17]. It is surprising to note that the GBSM approach has not yet been used for UAV channel modeling.

In this paper, we for the first time apply the GBSM approach to UAV-MIMO channel modeling and propose a novel 3D GBSM. It is assumed that all the effective scatterers around the ground mobile user are distributed on the surface of a cylinder, while the UAV is free of scatterers. Based on this model, we derive the theoretical expression of the STCF and investigate the impact of several unique UAV-related parameters on STCFs, e.g., the elevation angle and moving direction of the UAV. Numerical results have shown some interesting and useful observations. Finally, the close agreement between the obtained theoretical temporal correlation and the measurement data in [9] demonstrates the usefulness of our model.

The remainder of this paper is organized as follows. Section II describes a UAV-MIMO communication system. In Section III, we introduce the 3D GBSM for UAV-MIMO channels, and then derive the STCF based on this model. Section IV shows numerical results and conclusions are drawn in Section V.

II. Communication System Based on UAV

The system model in this paper is investigating a UAV-MIMO air-to-ground (A2G) communication channel with n_T

978-1-5090-4183-1/17/$31.00 ©2017 IEEE

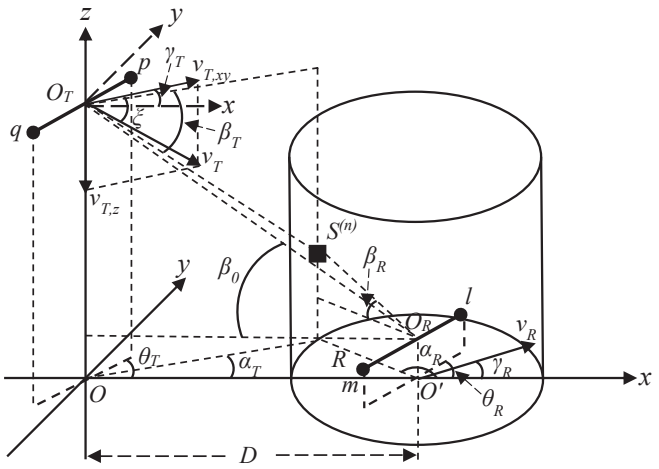

Fig. 1. A 3D GBSM for UAV-MIMO channels.

transmit and n_R receive antenna elements, numbered as $1 \leq p \leq q \leq n_T$ and $1 \leq l \leq m \leq n_R$, respectively. The n_T transmit antenna elements belong to the transmitter (Tx, UAV) which suspends itself in the air, and the receiver (Rx, ground user) with n_R receive elements is assumed to move slowly.

Since the LoS components of A2G links are usually blocked by the tree crowns or buildings in urban areas, we only take non-LoS (NLoS) components into account in this model. The effective scatterers around the ground station are nonuniformly distributed, with a joint probability density function (PDF), on the surface of a cylinder (radius R and height H) centered at the Rx, while the scatterers around the UAV are neglected.

III. Three-Dimensional GBSM for UAV-MIMO Channels

In this section, we propose a 3D cylinder GBSM for UAV-MIMO channels and derive the STCF of the link between an aerial UAV and a terrestrial mobile user. Since the UAV can fly in a noticeable altitude, propagating electromagnetic waves are supposed to travel in a 3D space, which is why we need a 3D model.

Fig. 1 shows the NLoS paths in 2×2 UAV-MIMO channel. It is not difficult to further construct a uniform linear array with an arbitrary number of antenna elements. The two transmit antenna elements p and q are centered as O_T, which are H_T higher than the origin O, and the receive ones l and m are placed around O_R, lifted H_R up O'. To aid our statement, we denote $d(A, B)$ as the distance between two points A and B, e.g., $d(O, O') = D$, $d(O, O_T) = H_T$ and $d(O', O_R) = H_R$.

A general condition that $H_T \gg H_R$ can simplify the expression of the elevation angle β_0 of the UAV, relative to O_R

$$\beta_0 = \arctan \frac{H_T - H_R}{D} \approx \arctan \frac{H_T}{D}. \tag{1}$$

Some other assumptions are also exploited in the following derivations, e.g., $\delta_T, \delta_R \ll R \ll D$.

The spacing between two adjacent antenna elements on the UAV (or on the ground station) is defined as δ_T (or δ_R). Besides, the orientations of two antenna arrays are denoted by θ_T and θ_R relative to the x-axis, respectively. The two stations are moving with velocities v_T and v_R. Without loss of generality, we assume that the UAV is descending. In this paper, we for the first time introduce an angle pair, ξ and γ_T, to describe the movement of the UAV in a 3D space. As shown in Fig. 1, we decompose the vector v_T into a horizontal component $v_{T,xy}$ and a perpendicular component $v_{T,z}$. Then, we define $\langle v_{T,xy}, v_T \rangle = \xi$, and $\langle v_{T,xy}, +x \rangle = \gamma_T$, where $\langle \cdot, \cdot \rangle$ denotes the included angle. The movement of the ground user is in the xy plane with the direction of $\langle v_R, +x \rangle = \gamma_R$.

Assuming the nth scatterer is denoted by $S^{(n)}$, we define the azimuth and the elevation angle of the Tx's center O_T, relative to $S^{(n)}$, as $\alpha_T^{(n)}$ and $\beta_T^{(n)}$, which are also called the angles of departure (AoD). Similarly, the angles of arrival (AoA) represent the azimuth and the elevation angle of $S^{(n)}$ relative to O_R (approximately O') respectively, denoted by $\alpha_R^{(n)}$ and $\beta_R^{(n)}$. According to some geometrical relations, we can figure out the dependence between $\alpha_T^{(n)}$, $\beta_T^{(n)}$ and $\alpha_R^{(n)}$, $\beta_R^{(n)}$. The derivation will be addressed later. In fact, the parameters $\alpha_R^{(n)}$, $\beta_R^{(n)}$ also characterize the distribution of local scatterers. Other significant parameters are listed and defined in Table I.

Above all, we write down the expression of the channel impulse response (CIR). Note that the LoS path is not expected to exist, so the CIR between antenna elements p and l is

$$\begin{aligned} h_{pl}(t) = &\sqrt{\Omega_{pl}} \lim_{N\to\infty} \frac{1}{\sqrt{N}} \sum_{n=1}^{N} e^{j\phi(n)} e^{-j\frac{2\pi}{\lambda}[d(p,S^{(n)})+d(S^{(n)},l)]} \\ &e^{j2\pi f_T t[\cos(\alpha_T^{(n)}-\gamma_T)\cos\beta_T^{(n)}\cos\xi+\sin\beta_T^{(n)}\sin\xi]} \\ &e^{j2\pi f_R t[\cos(\alpha_R^{(n)}-\gamma_R)\cos\beta_R^{(n)}]} \cdot g^{(n)} \end{aligned} \tag{2}$$

where $j^2 = -1$, λ is the carrier wavelength, $f_T = v_T/\lambda$ and $f_R = v_R/\lambda$ are maximum Doppler shifts. In addition, $g^{(n)}$ represents the amplitude of the nth scattered wave such that $\lim_{N\to\infty} \sum_{n=1}^{N} \mathrm{E}[|g^{(n)}|^2] = 1$, where N is the number of scatterers.

TABLE I
Definition of Significant Parameters in the Model

Symbol	Definition
D	The horizontal distance between Tx and Rx
R	The radius of the effective-scatterer cylinder
β_0	The elevation angle of the UAV's location
H_T, H_R	The height of Tx and Rx, respectively
δ_T, δ_R	The spacing between antenna elements at Tx and Rx
θ_T, θ_R	The orientation of antenna arrays at Tx and Rx
v_T, v_R	The velocity of Tx and Rx, respectively
$v_{T,xy}$, $v_{T,z}$	The horizontal and the perpendicular component of v_T
f_T, f_R	The maximum Doppler shift caused by Tx and Rx
ξ	The angle between two vectors $\langle v_{T,xy}, v_T \rangle$
γ_T, γ_R	The angle $\langle v_{T,xy}, +x \rangle$ and $\langle v_R, +x \rangle$, respectively
$\alpha_T^{(n)}$, $\beta_T^{(n)}$	The azimuth and elevation AoD at $S^{(n)}$
$\alpha_R^{(n)}$, $\beta_R^{(n)}$	The azimuth and elevation AoA from $S^{(n)}$
$g^{(n)}$, $\phi^{(n)}$	The amplitude gain and random phase by $S^{(n)}$
α_μ, k	The parameters in von-Mises PDF of the azimuth AoA
β_μ, β_m	The parameters in cosine PDF of the elevation AoA
$d(A, B)$	The abbreviation for the distance between A and B

Now we derive the STCF of the complex faded envelope of two arbitrary subchannels pl and qm. It is defined as

$$R_{pl,qm}(\delta_T, \delta_R, \tau, t) = \frac{\mathrm{E}[h^*_{pl}(t) h_{qm}(t+\tau)]}{\sqrt{\Omega_{pl}\Omega_{qm}}} \tag{3}$$

where $h_{pl}(t)$ and $h_{qm}(t)$ denote the CIRs of subchannels pl and qm, respectively. Provided that the channel is a stationary random process, the expression (3) can be written as

$$\begin{aligned} &R_{pl,qm}(\delta_T, \delta_R, \tau, t) = R_{pl,qm}(\delta_T, \delta_R, \tau) \\ &= \lim_{N\to\infty} \frac{1}{N} \sum_{n=1}^{N} \mathrm{E}[|g^{(n)}|^2 e^{j2\pi f_R \tau [\cos(\alpha_R^{(n)} - \gamma_R)\cos\beta_R]} \\ &\quad e^{j2\pi f_T \tau [\cos(\alpha_T^{(n)} - \gamma_T)\cos\beta_T^{(n)}\cos\xi + \sin\beta_T^{(n)}\sin\xi]} \\ &\quad e^{-j\frac{2\pi}{\lambda}[d(p,S^{(n)}) + d(S^{(n)},l)] - [d(q,S^{(n)}) + d(S^{(n)},m)]}]. \end{aligned} \tag{4}$$

Based on geometrical relations of this single-bounce model, we can obtain the dependence between angles $\alpha_T^{(n)}$, $\beta_T^{(n)}$ and $\alpha_R^{(n)}$, $\beta_R^{(n)}$. Since $R \ll D$, the angle α_T is extremely small. By applying the law of sines in relevant triangles, we have

$$\cos\alpha_T^{(n)} \approx 1, \sin\alpha_T^{(n)} \approx \frac{\frac{R}{D}\sin\alpha_R^{(n)}}{1 + \frac{R}{D}\cos\alpha_R^{(n)}}. \tag{5}$$

Along the z-axis, we have

$$D\tan\beta_0 = (D + R\cos\alpha_R^{(n)})\tan\beta_T^{(n)} + R\tan\beta_R^{(n)} \tag{6}$$

i.e.,

$$\tan\beta_T^{(n)} = \frac{D\tan\beta_0 - R\tan\beta_R^{(n)}}{D + R\cos\alpha_R^{(n)}} = \frac{\tan\beta_0 - \frac{R}{D}\tan\beta_R^{(n)}}{1 + \frac{R}{D}\cos\alpha_R^{(n)}} \tag{7}$$

and considering some approximate relations, e.g., $\sqrt{1+x} \approx 1 + \frac{1}{2}x$, if $x \ll 1$, we can obtain the approximate expressions

$$\begin{aligned} \cos\beta_T^{(n)} &\approx \cos\beta_0[1 + \frac{R}{D}\sin^2\beta_0\cos\beta_0(\frac{\tan\beta_R^{(n)}}{\sin\beta_0} + \frac{\cos\alpha_R^{(n)}}{\cos\beta_0})] \\ \sin\beta_T^{(n)} &\approx \sin\beta_0[1 - \frac{R}{D}\cos^2\beta_0\cos\beta_0(\frac{\tan\beta_R^{(n)}}{\sin\beta_0} + \frac{\cos\alpha_R^{(n)}}{\cos\beta_0})]. \end{aligned} \tag{8}$$

The number of scatterers is infinite in this model. Therefore, discrete random variables $\alpha_R^{(n)}$ and $\beta_R^{(n)}$ can be replaced with continuous random variables α_R and β_R. If the two random variables are independent, the joint PDF $f(\alpha_R, \beta_R)$ can be decomposed to $f(\alpha_R)f(\beta_R)$. Hence, the correlation function becomes

$$\begin{aligned} &R_{pl,qm}(\delta_T, \delta_R, \tau, t) = R_{pl,qm}(\delta_T, \delta_R, \tau) \\ &= \int_{\beta_{R1}}^{\beta_{R2}} \int_{-\pi}^{\pi} e^{-j\frac{2\pi}{\lambda}[d(p,S^{(n)}) + d(S^{(n)},l)] - [d(q,S^{(n)}) + d(S^{(n)},m)]} \\ &\quad e^{j2\pi f_T \tau [\cos(\alpha_T - \gamma_T)\cos\beta_T\cos\xi + \sin\beta_T\sin\xi]} \\ &\quad e^{j2\pi f_R \tau [\cos(\alpha_R - \gamma_R)\cos\beta_R]} f(\alpha_R) f(\beta_R) \mathrm{d}\alpha_R \mathrm{d}\beta_R. \end{aligned} \tag{9}$$

In this paper, we use the von Mises PDF to characterize the azimuth angle α_R. The von Mises PDF is defined as

$$f(\alpha_R) = \frac{e^{k\cos(\alpha_R - \alpha_\mu)}}{2\pi I_0(k)}, -\pi \le \alpha_R \le \pi \tag{10}$$

where $I_0(\cdot)$ is the zeroth-order modified Bessel function of the first kind, and $\alpha_\mu \in [-\pi, \pi]$ is the mean angle at which the scatterers are distributed in the xy plane. The parameter k controls the spread around the mean angle. Setting $k = 0$ incurs isotropic scattering, i.e., $f(\alpha_R) = \frac{1}{2\pi}, \alpha_R \in [-\pi, \pi]$, and the scattering becomes more non-isotropic as k increases.

The elevation angle β_R is described as the cosine PDF, with two parameters β_μ and β_m related to the mean angle and variance, respectively. The cosine PDF is

$$f(\beta_R) = \frac{\pi}{4\beta_m}\cos(\frac{\pi}{2}\frac{\beta_R - \beta_\mu}{\beta_m}), |\beta_R - \beta_\mu| \le \beta_m \le \frac{\pi}{2}. \tag{11}$$

To obtain the results of STCFs, the integral of (9) has to be numerically evaluated, since there is no closed-form solution.

IV. Numerical Results and Analysis

In this section, the STCFs of UAV-MIMO channels are numerically analyzed by changing model parameters. In addition, some of the theoretical results are compared with the measurement data in [9]. Unless indicated otherwise, the values of the parameters used for our numerical analysis are $n_T = n_R = 2$, $\beta_0 = \pi/3$, $R = 20\mathrm{m}$, $D = 1000\mathrm{m}$, $\lambda = 0.1\mathrm{m}$, $v_T = 10\mathrm{m/s}$, $v_R = 0.1\mathrm{m/s}$, $\gamma_T = \pi/4$, $\gamma_R = \pi/3$, $\xi = \pi/24$, $\alpha_\mu = \pi$, $k = 3$, $\beta_\mu = \pi/4$, $\beta_m = \pi/6$, and $\theta_T = \theta_R = \pi/2$.

Fig. 2 shows the temporal correlations $R_{pl}(\tau)$ for different moving directions of the UAV. To highlight the impact of the UAV's movement, we minimize the velocity of the ground mobile user to $v_R = 0.01\mathrm{m/s}$ with $\gamma_R = 0$. It can be observed from Fig. 2 that the maximum temporal correlation emerges when the UAV is moving straight towards the quasi-stationary ground mobile user, i.e., $\xi = \beta_0 = \pi/3$ and $\gamma_T = 0$. Compared with other movement directions, when the UAV is moving straight towards the ground mobile user, the change of the propagation environment is the smallest, resulting in the maximum temporal correlation under this UAV moving direction. This interesting observation suggests that the UAV should move towards the ground mobile user for reliable UAV communication performance.

Fig. 3 depicts the temporal correlations $R_{pl}(\tau)$ for different elevation angles β_0 of the UAV's location. From Fig. 3, it is clear that the higher the β_0, the higher the temporal correlation under a non-isotropic environment. It is because that increasing β_0 increases the distance between the UAV and the ground mobile user, i.e., $d(\mathrm{Tx}, \mathrm{Rx}) = D/\cos\beta_0$. The larger the distance $d(\mathrm{Tx}, \mathrm{Rx})$, the smaller the impact of UAV movement. Therefore, the larger the β_0, the higher the temporal correlation.

Fig. 4 presents the transmit spatial correlations $R_{pl,ql}(\delta_T)$ for different distributions of local scattering in the azimuth domain, which is controlled by the parameter k of the von Mises distribution. The larger the parameter k, the more concentrated the local scattering in the azimuth domain, and thus the smaller the angle spread, which results in the higher spatial correlation.

Fig. 5 illustrates the comparison of the transmit STCF $R_{pl,ql}(\delta_T, \tau)$ for two different UAV movement directions with

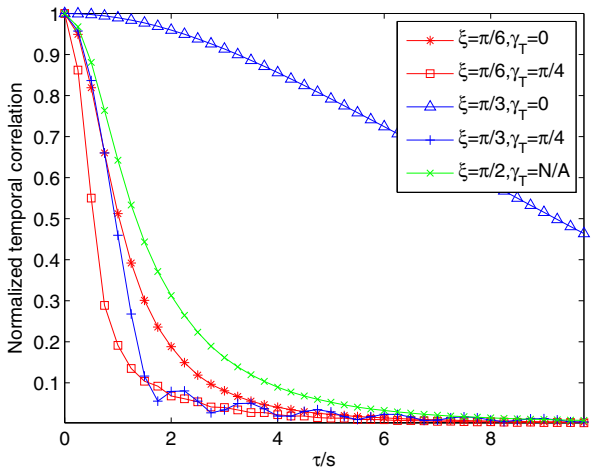

Fig. 2. Temporal correlations for different moving directions of the UAV.

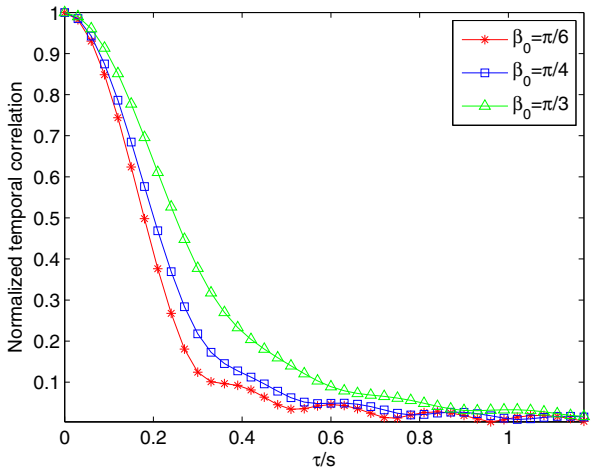

Fig. 3. Temporal correlations for different elevation angles of the UAV.

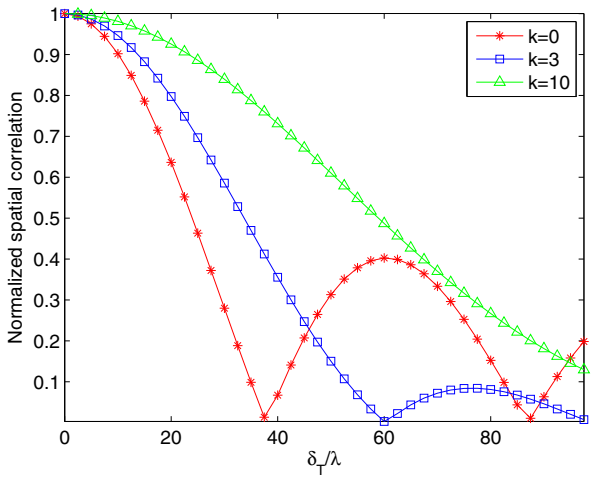

Fig. 4. Transmit spatial correlations for different spreads of scatterers.

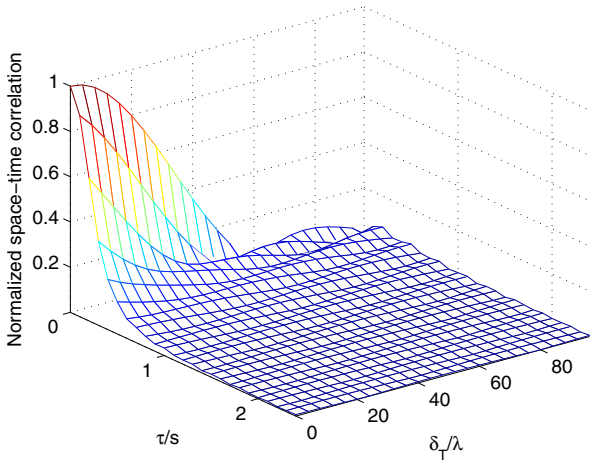

(a)

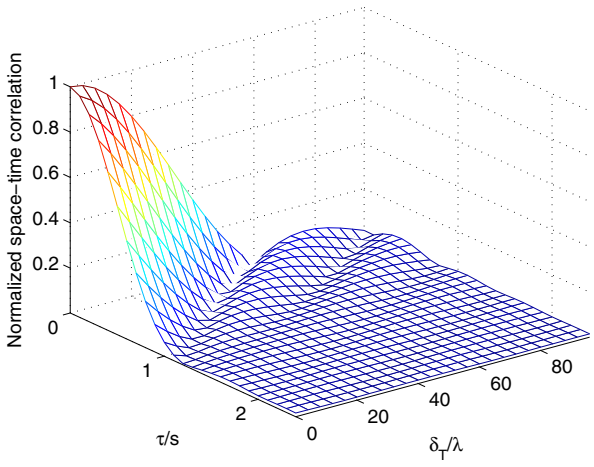

(b)

Fig. 5. Transmit space-time correlations for (a) UAV horizontal movement ($\xi = 0$) and (b) UAV vertical movement ($\xi = \pi/2$).

the values of $\xi = 0$ (horizontal movement) and $\xi = \pi/2$ (vertical movement). From Fig. 5, it is clear that the fluctuation of space-time correlation is serious when UAV is moving vertically. This interesting observation suggests that the UAV should move horizontally for reliable MIMO performance.

Fig. 6 shows the spatial correlation $R_{pl,qm}(\delta_T, \delta_R)$ under a non-isotropic scattering environment. From Fig. 6, we can observe that the space correlation at the Rx is smaller than the one at the Tx. It is because that our model assumes all scatterers are around the Rx and the Tx is free of scatterers.

Fig. 7 presents the comparison between theoretical results and some measurement data. Based on a measurement in urban areas for UAV channels (approximately Rayleigh fading) [9], we choose the following parameters: $\beta_0 = \pi/10$, $R = 100\text{m}$, $D = 1000\text{m}$, $\lambda = 0.15\text{m}$, $v_T = 8\text{m/s}$, $v_R = 0$, $\gamma_T = \pi/11$, $\xi = 0$, $\alpha_\mu = \pi$, $k = 0.5$, and $\beta_\mu = \beta_m = \pi/10$. The excellent agreement in Fig. 7 justifies the proposed model.

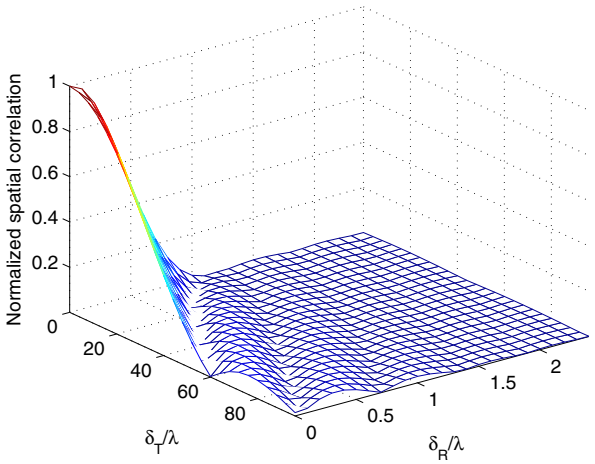

Fig. 6. Spatial correlation under a non-isotropic environment.

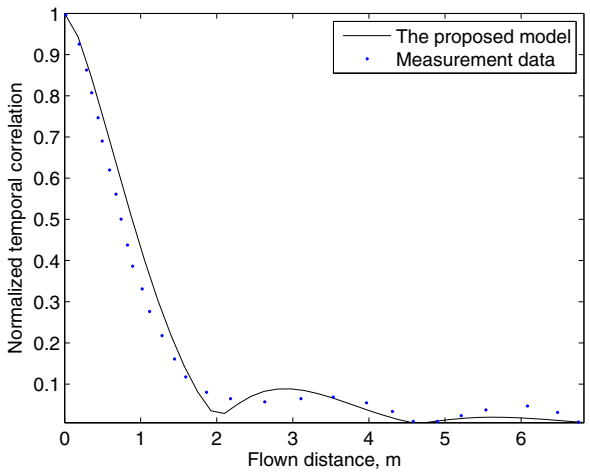

Fig. 7. Comparison between the theoretical results and the measurement data. (Note that the correlation time were replaced by the flown distance.)

V. Conclusions

In this paper, we have proposed a 3D cylinder GBSM for UAV-MIMO Rayleigh channels and investigated the impact of some unique UAV-related parameters, e.g., the UAV's moving directions. Numerical results have shown that some important parameters, e.g., UAV movement direction and UAV location, have great impact on the resulting correlations. Among these numerical results, several interesting observations suggest that the UAV should move towards the ground mobile user in order to maintain a stable UAV link, while for obtaining reliable MIMO performance, the UAV should move horizontally. Finally, the observation that the theoretical results matched the measurement data validates the usefulness of our model.

VI. Acknowledgment

This work was jointly supported by the National Natural Science Foundation of China (Grant No. 61622101, 61571020, and 61471268), the National 973 project (Grant No. 2013CB336700), the open research fund of National Mobile Communications Research Laboratory, Southeast University (Grant No. 2016D03), the 863 Project in 5G (Grant No. 2014AA01A701), EU H2020 ITN 5G Wireless project (Grant No. 641985), EU FP7 QUICK project (Grant No. PIRSES-GA-2013-612652), and EPSRC TOUCAN project (Grant No. EP/L020009/1).

References

[1] Y. Zeng, R. Zhang, and T. J. Lim, "Wireless communications with unmanned aerial vehicles: opportunities and challenges," *IEEE Commun. Mag.*, vol. 54, no. 5, pp. 36–42, May 2016.

[2] D. W. Matolak, "Air-ground channels & models: Comprehensive review and considerations for unmanned aircraft systems," in *Proc. IEEE Aerospace Conf.*, Big Sky, MT, USA, Mar. 2012, pp. 1–17.

[3] E. Yanmaz, R. Kuschnig, and C. Bettstetter, "Channel measurements over 802.11a-based uav-to-ground links," in *Proc. IEEE GLOBECOM Workshops*, Houston, TX, USA, Dec. 2011, pp. 1280–1284.

[4] D. Matolak and R. Sun, "Air-ground channel measurements and modeling for uas," *IEEE Aerosp. Electron. Syst. Mag.*, vol. 29, no. 11, pp. 30–35, Nov. 2014.

[5] K. Takizawa, T. Kagawa, S. Lin, F. Ono, H. Tsuji, and R. Miura, "C-band aircraft-to-ground (a2g) radio channel measurement for unmanned aircraft systems," in *Proc. WPMC*, Sydney, Australia, Sept. 2014, pp. 754–758.

[6] J. Romeu, A. Aguasca, J. Alonso, S. Blanch, and R. R. Martins, "Small uav radiocommunication channel characterization," in *Proc. EuCAP*, Barcelona, Spain, Apr. 2010, pp. 1–5.

[7] K. Daniel, M. Putzke, B. Dusza, and C. Wietfeld, "Three dimensional channel characterization for low altitude aerial vehicles," in *Proc. ISWCS*, York, United Kingdom, Sept. 2010, pp. 756–760.

[8] Z. Shi, P. Xia, Z. Gao, L. Huang, and C. Chen, "Modeling of wireless channel between uav and vessel using the fdtd method," in *Proc. WiCOM*, Beijing, China, Sept. 2014, pp. 100–104.

[9] M. Simunek, F. P. Fontán, and P. Pechac, "The uav low elevation propagation channel in urban areas: Statistical analysis and time-series generator," *IEEE Trans. Antennas Propag.*, vol. 61, no. 7, pp. 3850–3858, Jul. 2013.

[10] D. W. Matolak and R. Sun, "Unmanned aircraft systems: Air-ground channel characterization for future applications," *IEEE Veh. Technol. Mag.*, vol. 10, no. 2, pp. 79–85, Jun. 2015.

[11] X. Yin and X. Cheng, *Propagation Channel Characterization, Parameter Estimation, and Modeling for Wireless Communications*. Wiley-IEEE Press, 2016.

[12] A. G. Zajić and G. L. Stüber, "Three-dimensional modeling, simulation, and capacity analysis of space-time correlated mobile-to-mobile channels," *IEEE Trans. Veh. Technol.*, vol. 57, no. 4, pp. 2042–2054, Jul. 2008.

[13] X. Cheng, C. X. Wang, D. I. Laurenson, S. Salous, and A. V. Vasilakos, "An adaptive geometry-based stochastic model for non-isotropic mimo mobile-to-mobile channels," *IEEE Trans. Wireless Commun.*, vol. 8, no. 9, pp. 4824–4835, Sept. 2009.

[14] Y. Yuan, C. X. Wang, X. Cheng, B. Ai, and D. I. Laurenson, "Novel 3d geometry-based stochastic models for non-isotropic mimo vehicle-to-vehicle channels," *IEEE Trans. Wireless Commun.*, vol. 13, no. 1, pp. 298–309, Jan. 2014.

[15] X. Cheng, C. X. Wang, H. Wang, X. Gao, X. H. You, D. Yuan, B. Ai, Q. Huo, L. Y. Song, and B. L. Jiao, "Cooperative mimo channel modeling and multi-link spatial correlation properties," *IEEE J. Sel. Areas Commun.*, vol. 30, no. 2, pp. 388–396, Feb. 2012.

[16] X. Cheng, Q. Yao, M. Wen, C. X. Wang, L. Y. Song, and B. L. Jiao, "Wideband channel modeling and intercarrier interference cancellation for vehicle-to-vehicle communication systems," *IEEE J. Sel. Areas Commun.*, vol. 31, no. 9, pp. 434–448, Sept. 2013.

[17] X. Cheng, C. X. Wang, B. Ai, and H. Aggoune, "Envelope level crossing rate and average fade duration of nonisotropic vehicle-to-vehicle ricean fading channels," *IEEE Trans. Intell. Transp. Syst.*, vol. 15, no. 1, pp. 62–72, Feb. 2014.